STELLAR EVOLUTION. IV. THE EVOLUTION OF A 9 $M_\odot$ STAR FROM THE MAIN SEQUENCE THROUGH CORE HELIUM BURNING*

ICKO IBEN, JR.†
California Institute of Technology, Pasadena, and
Massachusetts Institute of Technology, Cambridge

Received July 12, 1965

ABSTRACT

A 9 $M_\odot$ stellar model of population I initial composition ($X_H = 0.708$, $Z = 0.02$) is evolved from the main sequence to the stage of helium exhaustion in the core. Comparison is made with the evolution of the 3 $M_\odot$ and 5 $M_\odot$ models described in preceding papers of this series. Relative lifetimes for corresponding evolutionary phases and changes in evolutionary paths in the H-R diagram are found to vary in a consistent way with increasing stellar mass. The phase of rapid envelope contraction associated with the disappearance of envelope convection has much greater observational consequences in the 9 $M_\odot$ case than in the 5 $M_\odot$ case. Passage through the Cepheid strip occurs only once during core helium burning and then on a Kelvin-Helmholtz time scale. The core helium-burning phase is broken into two quite distinct phases, the second phase occurring at much higher surface temperatures than in the 5 $M_\odot$ case.

I. PRELIMINARY REMARKS

The discussion of 9 $M_\odot$ evolution is based on 665 models carried from the main sequence to the phase of helium exhaustion in the stellar core. Changes in initial composition characteristics during pre–main-sequence evolution are described in Paper I (Iben 1965*a*). The method of solution, the opacity, the equation of state, the treatment of convection, and the energy-generation laws employed are the same as in Papers I and II (Iben 1965*a*, *b*). Since 9 $M_\odot$ evolution is qualitatively quite similar to the evolution of the 3 $M_\odot$ and 5 $M_\odot$ stars described in Papers II and III (Iben 1966), emphasis is placed primarily on a presentation rather than on an interpretation of the calculational results.

II. OVER-ALL CHARACTERISTICS

The path in the Hertzsprung-Russell diagram of the 9 $M_\odot$ star is given in Figure 1. Times to reach labeled points may be found in Table 1 in units of 10^7 years. The variation with time of several internal and observable characteristics is given in Figures 2 and 3 for all evolutionary phases and also in Figure 7 (see below) for a shorter period of rapid evolutionary changes.

In columns (4) and (5) of Table 2 are the absolute and relative time intervals spent by the 9 $M_\odot$ star in each of several phases. Corresponding time intervals for 5 $M_\odot$ evolution are given in columns (2) and (3) of Table 2.

It is evident that, as stellar mass is increased, less time is spent in every phase following the development of the hydrogen-burning shell relative to time spent near the main sequence during core hydrogen burning. Further, with increasing stellar mass, the descent from the red-giant tip occupies a smaller fraction of the total core helium-burning lifetime.

After the descent from the red-giant tip, the phase of rapid envelope contraction associated with the disappearance of envelope convection breaks the period of core helium burning into two quite distinct phases (see curve R versus t in Fig. 3, and curves $\log (L)$ versus t and $\log (T_e)$ versus t in Fig. 2). This break is not evident in 3 $M_\odot$ evolution and becomes just discernible in 5 $M_\odot$ evolution.

* Supported in part by the Office of Naval Research (Nonr-220(47)) and the National Aeronautics and Space Administration (NGR-05-002-028 and NSG-496).

† Now at Massachusetts Institute of Technology.

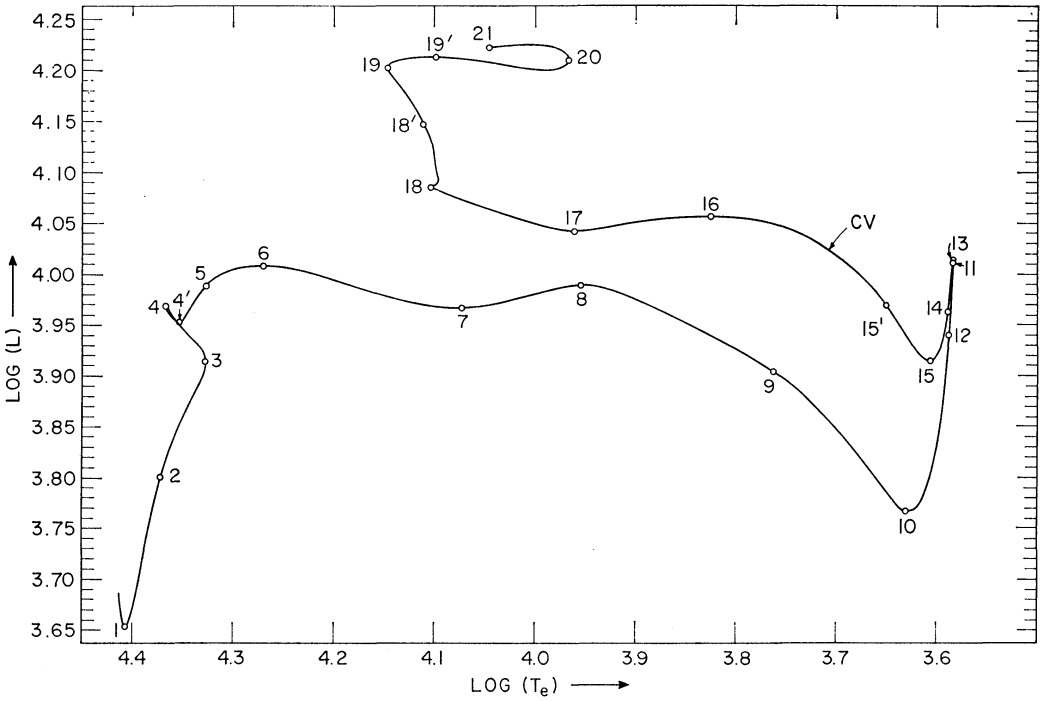

FIG. 1.—The path of a 9 $M_\odot$ population I star in the theoretical Hertzsprung-Russell diagram. Luminosity L is in units of 3.86×10^{33} ergs/sec and surface temperature T_e is in units of degrees Kelvin.

TABLE 1

EVOLUTIONARY LIFETIMES (10^7 YEARS)

Point	Time	Point	Time	Point	Time
1.....	0.0232171	9.....	2.212819	17.....	2.277173
2.....	1.435125	10.....	2.213585	18.....	2.314993
3.....	2.129274	11.....	2.214220	18′.....	2.455107
4.....	2.189700	12.....	2.215236	19.....	2.567444
4′.....	2.190826	13.....	2.220137	19′.....	2.607521
5.....	2.193710	14.....	2.243431	20.....	2.623007
6.....	2.198813	15.....	2.267412	21.....	2.625870
7.....	2.206125	15′.....	2.272310		
8.....	2.209479	16.....	2.273715		

TABLE 2

COMPARATIVE LIFETIMES (10^7 YEARS)

PHASE	DESCRIPTION (POINTS) (1)	5 $M_\odot$		9 $M_\odot$	
		Δt_i (2)	$100(\Delta t_i/\Delta t_{10})$ (3)	Δt_i (4)	$100(\Delta t_i/\Delta t_{10})$ (5)
1.....	To main sequence	0.05759	0.656	0.01511	0.576
2.....	Core hydrogen burning (∼1–3)	6.54041	74.5	2.11416	80.5
3.....	Over-all gravitational contraction (3–4)	0.22358	2.44	0.06053	2.30
4.....	Shell development (4–4′)	0.00421	0.048	0.00113	0.043
5.....	Thick hydrogen-burning shell (4′–6)	0.13297	1.51	0.00798	0.304
6.....	Shell narrowing (6–10)	0.07532	0.857	0.01477	0.561
7.....	To red-giant tip (10–13)	0.04857	0.553	0.00655	0.249
8.....	Descent from red-giant tip (13–15)	0.49320	5.61	0.04727	1.80
9.....	Helium-burning core+hydrogen-burning shell (13–end)	1.70785	19.4	0.40573	15.450
10.....	Total time from birth	8.79060	100.00	2.62587	100.00

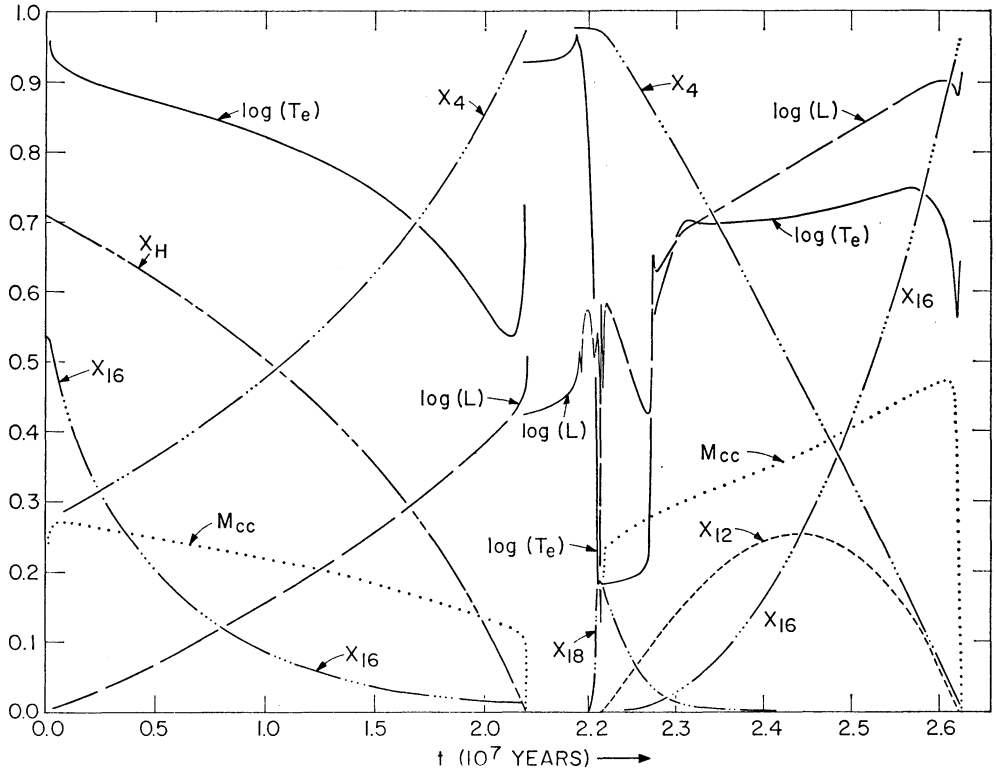

FIG. 2.—The variation with time t (units of 10^7 yr) of L, T_e, mass fraction in the convective core, M_{cc}, and central abundance by mass of $H^1(X_H)$, $He^4(X_4)$, $C^{12}(X_{12})$, $O^{16}(X_{16})$, and $O^{18}(X_{18})$. The unit of luminosity is $L_\odot = 3.86 \times 10^{33}$ ergs/sec and the unit of surface temperature is degrees Kelvin. To the left of the break in t, vertical scale limits correspond to $3.65 \leq \log(L) \leq 4.275$, $4.22 \leq \log(T_e) \leq 4.42$, $0 \leq M_{cc} \leq (\frac{1.9}{9})$, $0.0 \leq X_H, X_4 \leq 1.0$, and $0.0 \leq X_{14}, X_{16} \leq 0.02$. To the right of the break in t, scale limits correspond to $3.65 \leq \log(L) \leq 4.275$, $3.4 \leq \log(T_e) \leq 4.4$, $0.0 \leq M_{cc} \leq (\frac{2}{9})$, $0.0 \leq X_4, X_{12}, X_{16} \leq 1.0$, and $0.0 \leq X_{18} \leq 0.10$.

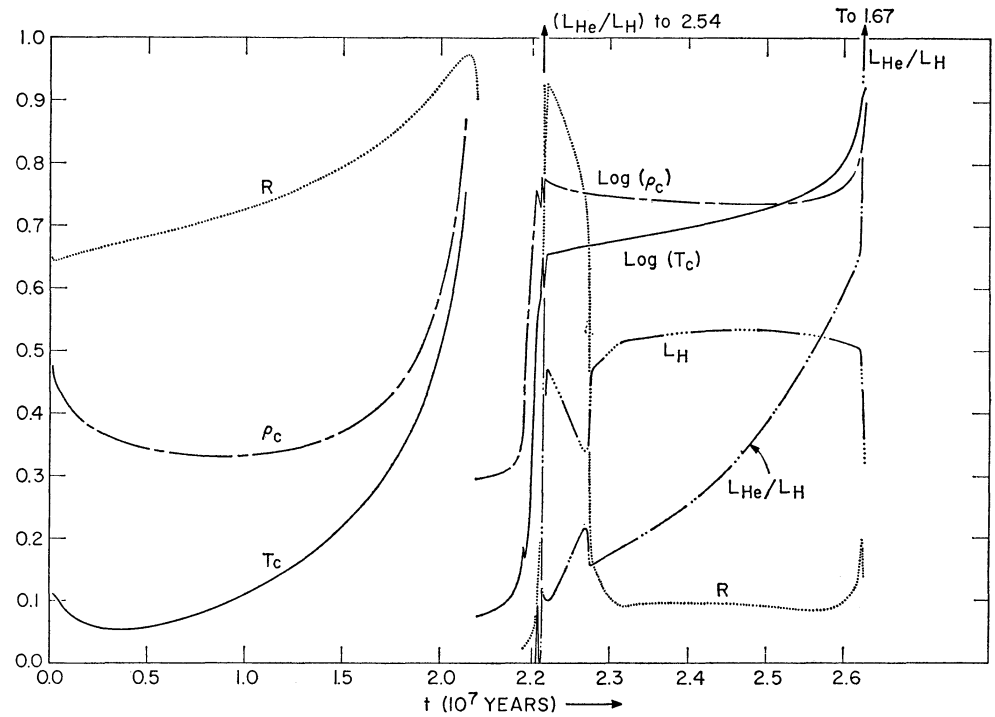

FIG. 3.—The variation with time t (units of 10^7 yr), of radius (R), central density (ρ_c), central temperature (T_c), the rate of energy production in the hydrogen-burning shell (L_H), and the rate of energy production by helium burning relative to the rate of energy production by hydrogen burning (L_{He}/L_H). Units are $R_\odot = 6.96 \times 10^{10}$ cm for radius, $10^{6\circ}$ K for temperature, gm/cm^3 for density, and $L_\odot = 3.86 \times 10^{33}$ ergs/sec for L_H. To the left of the break in t, scale limits correspond to $-3 \leq R \leq 7$, $6 \leq \rho_c \leq 16$, and $30 \leq T_c \leq 40$. To the right of the break in t, $0 \leq R \leq 250$, $0.7 \leq \log(\rho_c) \leq 4.7$, $1.5 \leq \log(T_c) \leq 2.5$, $0 \leq L_H \leq 20000$, and $0 \leq L_{He}/L_H \leq 1.0$.

III. FROM THE MAIN SEQUENCE TO THE FORMATION OF THE HYDROGEN-BURNING SHELL

The variation with mass fraction of state and composition variables within the star shortly after reaching the main sequence ($t = 4.08470 \times 10^5$ yr) is shown in Figure 4. As is to be expected, the convective core is much larger than in the 3 $M_\odot$ and 5 $M_\odot$ stars at comparable stages. C^{12} and He^3 are in average equilibrium in the core and in local equilibrium for a short distance beyond the core.

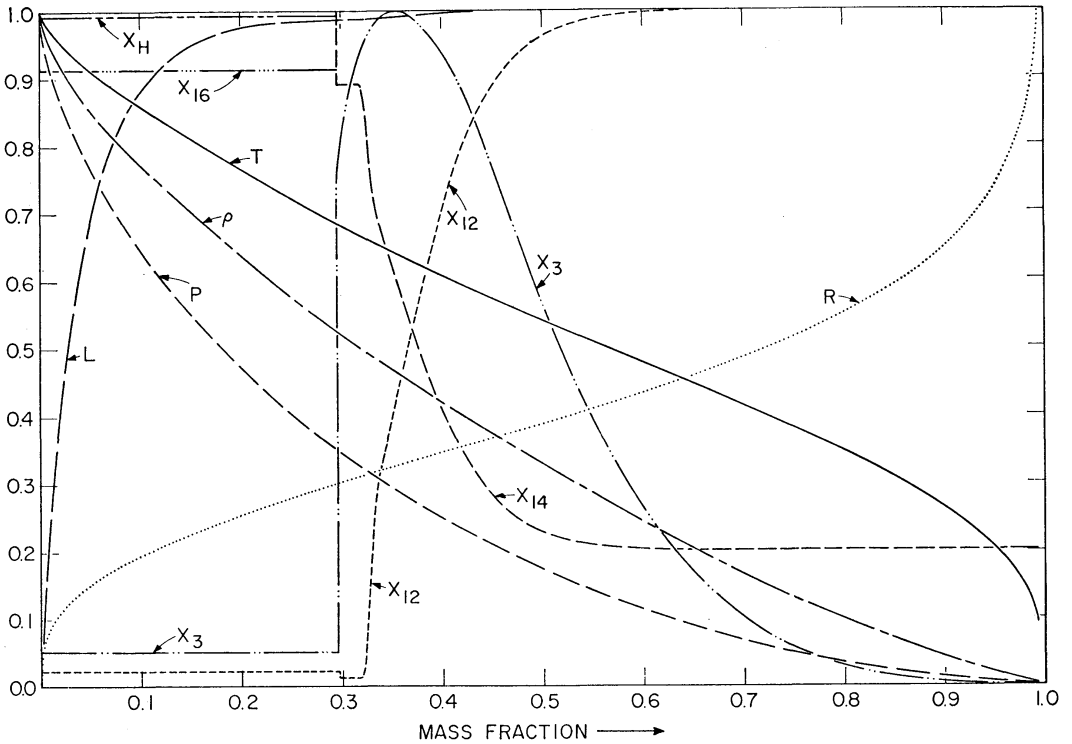

FIG. 4.—The variation with mass fraction of state and composition variables when $t = 4.08470 \times 10^5$ yr. Variables have the significance (and units): P = pressure (10^{17} dynes/cm^2), T = temperature ($10^{6\circ}$ K), ρ = density (gm/cm^3), L = luminosity (3.86×10^{33} ergs/sec), R = radius (6.96×10^{10} cm), X_i = abundance by mass of $H^1(X_H)$ $He^3(X_3)$, $C^{12}(X_{12})$, $N^{14}(X_{14})$, and $O^{16}(X_{16})$. Scale limits correspond to $0.0 \leq P \leq 0.455172$, $0.0 \leq T \leq 31.0141$, $0.0 \leq \rho \leq 10.3866$, $0.0 \leq L \leq 4503.90$, $0.0 \leq R \leq 2.68854$, $0.0 \leq X_H \leq 0.7080$, $0.0 \leq X_3 \leq 4.174 \times 10^{-6}$, $0.0 \leq X_{12} \leq 3.61 \times 10^{-3}$, $0.0 \leq X_{14} \leq 6.030 \times 10^{-3}$, and $0.0 \leq X_{16} \leq 1.080 \times 10^{-2}$. The mass fraction in the static envelope is 0.0020946, and the stellar radius is $R_s = 3.44875\ R_\odot$.

In the core, O^{16} is being converted slowly into N^{14}. From Figures 2 and 3 (curves ρ_c, T_c, and X_{14} versus t), it is evident that, just as in the 3 $M_\odot$ and 5 $M_\odot$ cases, central density and temperature drop during the early evolution from the main sequence as a result of the increase in core N^{14} abundance.

The period of over-all contraction begins near $t = 2.129 \times 10^7$ yr, when the central hydrogen abundance has been reduced to $X_H = 0.04$. The variation with time of pertinent stellar characteristics toward the end of the contractive phase is shown in Figure 7 (see below). As hydrogen is effectively exhausted in central regions, the fractional decrease in the rate of nuclear-energy production is greater in the 9 $M_\odot$ star than in the 5 $M_\odot$ star (see curves log (L_n) versus t in Fig. 7 and in Fig. 7 of Paper III). This is a consequence of the much larger region in the 9 $M_\odot$ star over which the core source of nuclear energy decreases rapidly. The mass fraction in the convective core of the 9 $M_\odot$ star decreases slowly from $M_{cc} \backsim 0.30$ near the main sequence to $M_{cc} \backsim 0.12$, before retreat-

ing rapidly during the phases of gravitational contraction and shell development. The convective core in the 5 $M_\odot$ star decreases from $M_{cc} \backsim 0.22$ to $M_{cc} \backsim 0.08$ over the corresponding interval.

During the period of shell development, $t = 2.189 \times 10^7$ yr to $t = 2.191 \times 10^7$ yr, the outward energy flux becomes so large that matter in two regions between the shell and the surface becomes unstable against convection. This does not occur in the 3 $M_\odot$ and 5 $M_\odot$ stars, where the contraction rate and flux increase in the vicinity of the developing shell are less pronounced. The variation with time of the inner and outer boundaries of the larger of the two convective layers is given by the curves labeled M_{CI} and M_{CO} in Figure 7.

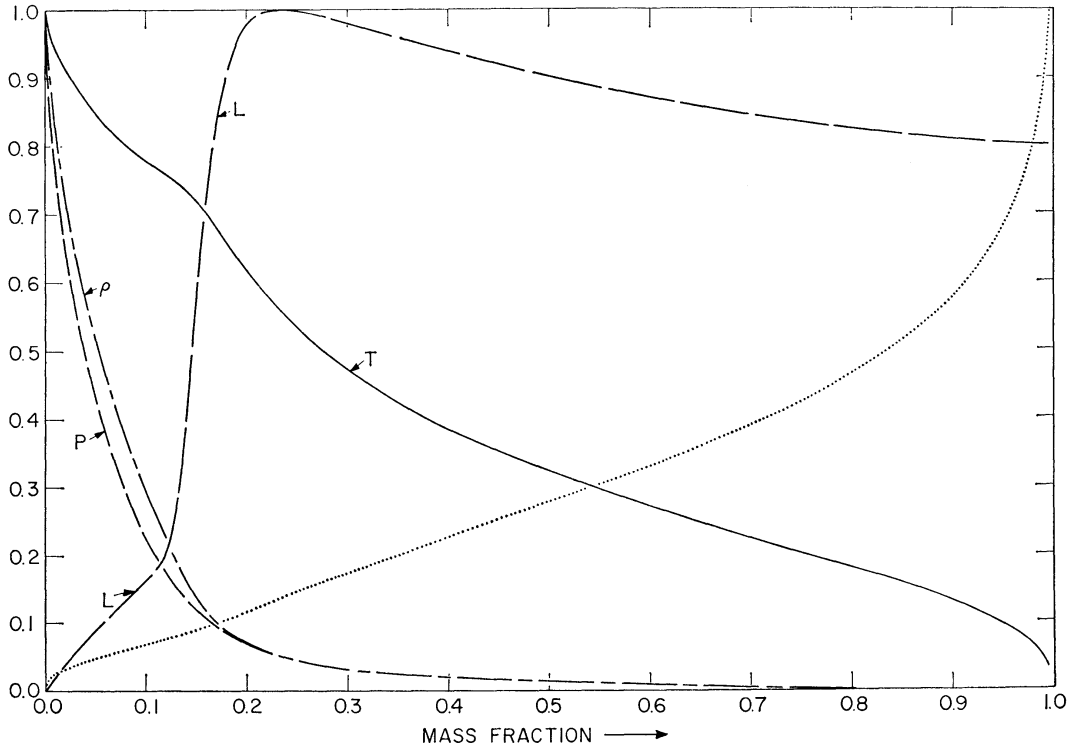

FIG. 5.—The variation with mass fraction of state variables when $t = 2.19029 \times 10^7$ yr. Variables have the same significance and physical units as in Fig. 4. Scale limits correspond to $0.0 \leq P \leq 1.95056$, $0.0 \leq T \leq 47.2258$, $0.0 \leq \rho \leq 62.6463$, $0.0 \leq L \leq 10899.2$, and $0.0 \leq R \leq 4.46786$. The mass fraction in the static envelope is 0.0020946, and the stellar radius is $R_s = 6.02823\ R_\odot$.

The distribution of state and composition variables within the star at $t = 2.19029 \times 10^7$ yr, just before the major convective layer reaches its maximum size, is exhibited in Figures 5 and 6. The central hydrogen abundance is $X_H = 2.77 \times 10^{-7}$ and the nuclear-energy production rate at the center is 9.252×10^{-3} times the rate of release of gravitational and thermal energy. Most of the energy produced in the region between the stellar center and the shell comes from the gravitational field ($L_g' \backsim 1650\ L_\odot$). The shell itself releases energy at the rate $L_H \backsim 9250\ L_\odot$. Energy absorbed in the expanding envelope is considerable, occurring at a rate $L_{abs} \backsim 1780\ L_\odot$. Matter interior to mass fraction 0.306 is moving inward and matter beyond is moving outward. Inward of mass fraction 0.188, density is increasing. Beyond this mass fraction, density is decreasing. Between mass fraction 0.018 and 0.413, temperatures are rising; elsewhere they are dropping.

The two convective regions are distinguished by the discontinuities in the abundance

distributions in Figure 6. They occur between mass fractions 0.2059 and 0.2846 and mass fractions 0.3217 and 0.3337, respectively. The larger convective layer, through which energy flux is still increasing, has not yet reached its maximum size, and the smaller layer, through which energy flux is decreasing, has begun to diminish in size.

The occurrence of two convective layers may be the result of a coarse treatment of convection, which ignores the possibility of semiconvection. It is possible that only one truly convective layer will appear during the period of shell development in a real 9 $M_\odot$ star.

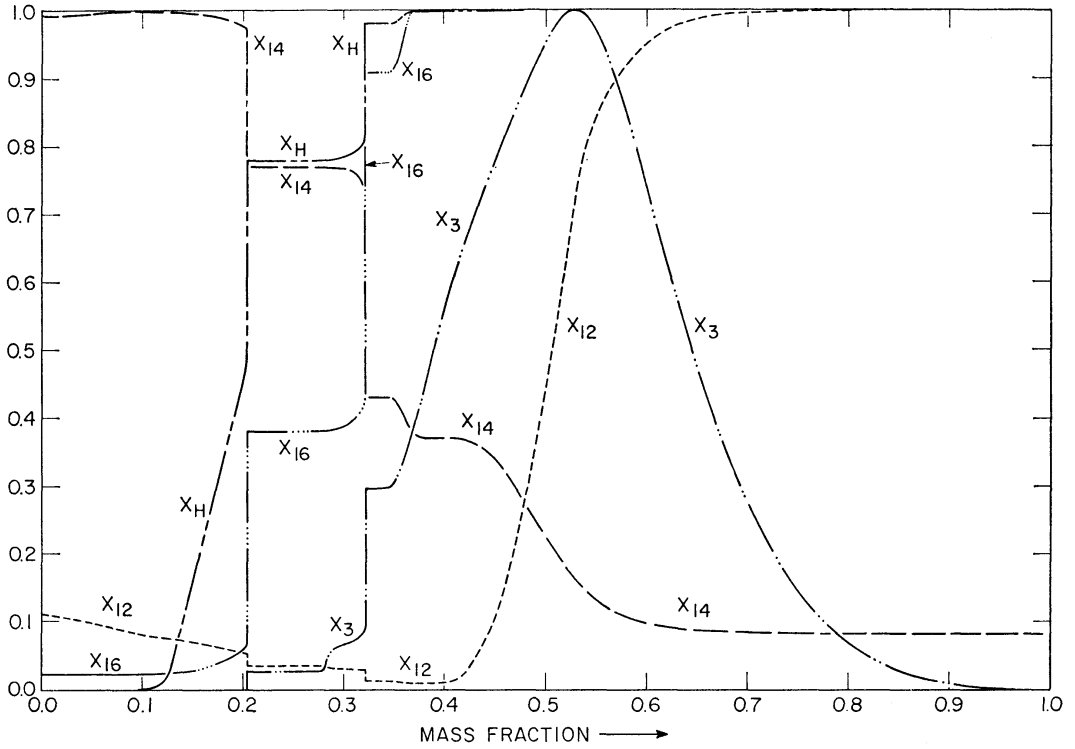

FIG. 6.—The variation with mass fraction of composition variables when $t = 2.19029 \times 10^7$ yr. Variables have the same significance and physical units as in Fig. 4. Scale limits correspond to $0.0 \leq X_H \leq 0.7080$, $0.0 \leq X_3 \leq 4.202 \times 10^{-5}$, $0.0 \leq X_{12} \leq 3.61 \times 10^{-3}$, $0.0 \leq X_{14} \leq 1.443 \times 10^{-2}$, and $0.0 \leq X_{16} \leq 1.080 \times 10^{-2}$. Convection occurs in two layers bounded by mass fraction $0.2059 \leq M_{l1} \leq 0.2846$ and $0.3217 \leq M_{l2} \leq 0.3337$.

The redistribution of N^{14} brought about by convection outside the shell has the effect of enhancing the increase in the surface ratio of N^{14} to C^{12} achieved near the red-giant tip. N^{14}, originating from the conversion of O^{16}, is convected from its place of origin to larger mass fractions, where temperatures are too low for this conversion to occur directly.

During the core hydrogen-burning phase, the conversion of both O^{16} and C^{12} into N^{14} has extended over larger interior mass fractions than in 3 $M_\odot$ and 5 $M_\odot$ stars. The center of the $C^{12} \rightarrow N^{14}$ transition layer (where one-half of the original C^{12} has been converted into N^{14}) is located at mass fraction 0.506 (see X_{12} in Fig. 6). This is to be compared with mass fractions of 0.445 and 0.466 found in the 3 $M_\odot$ and 5 $M_\odot$ cases, respectively, at the same stage of evolution. The depletion of Li has not been calculated.

The temperature gradient between the stellar center and the base of the developing shell, shown in Figure 5, is steeper than in the 3 $M_\odot$ and 5 $M_\odot$ stars at the same stage. This is partly due to the higher temperatures and lower densities in the 9 $M_\odot$ case (degeneracy and electron conduction play a less important role) and partly due to the fact that the rate at which gravitational energy is released in the core remains higher.

Contrary to the 3 $M_\odot$ and 5 $M_\odot$ cases, the hydrogen-depleted core does not even approach isothermal conditions. After only a brief drop during the shell-development stage, central temperature begins to rise again (see log (T_c) versus t in Fig. 7).

IV. TO THE RED-GIANT TIP

The formation of the hydrogen-burning shell is essentially complete when $t \backsim 2.191 \times 10^7$ yr. During the entire period of hydrogen burning in a thick shell (points 4′ to 6 in

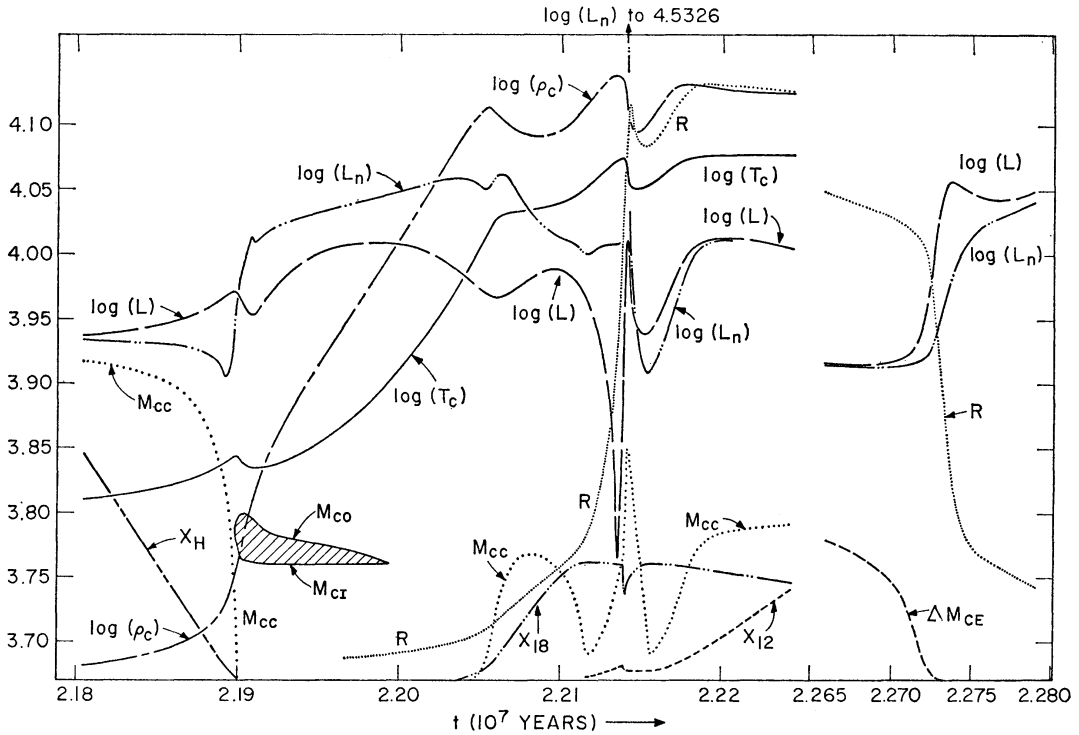

FIG. 7.—The variation with time t (10^7 yr.) of central density (ρ_c), central temperature (T_c), luminosity (L), rate of nuclear-energy production (L_n), stellar radius (R), mass fraction in the convective core (M_{cc}), mass fractions bounding the major convective layer (M_{CO} and M_{CI}), mass fraction in the convective envelope (ΔM_{CE}), and abundances by mass of $H^1(X_H)$, $O^{18}(X_{18})$, and $C^{12}(X_{12})$. Physical units for T_c, ρ_c, L, and R are the same as in Figs. 2 and 3. L_n has the same units as L. Scale limits correspond to $1.25 \leq \log(\rho_c) \leq 3.75$, $1.34 \leq \log(T_c) \leq 2.34$, $3.67 \leq \log(L) \leq 4.17$, $\log(L_n) \leq 4.17$, $0 \leq R \leq 250$, $0 \leq M_{cc} \leq (\frac{2}{3})$, $0 \leq M_{CO}, M_{CI} \leq (\frac{2}{3})$, $0 \leq \Delta M_{CE} \leq 1$, $0.0 \leq X_H \leq 0.02$, $0.0 \leq X_{12}, X_{18} \leq 0.1$.

Fig. 1), absorption in the expanding envelope remains considerable (see log (L) versus t and log (L_n) versus t in Fig. 7). During this phase in the 3 $M_\odot$ and 5 $M_\odot$ stars, envelope absorption remains much smaller relative to nuclear-energy production.

The conversion of N^{14} into O^{18} occurs at an earlier point in the evolutionary path (in the H-R diagram) of the 5 $M_\odot$ star than it occurs in the path of the 3 $M_\odot$ star. Central temperatures in the 9 $M_\odot$ star reach sufficiently high values to fire the $N^{14}(\alpha,\gamma)F^{18}(\beta^+\nu)O^{18}$ reactions shortly after the termination of thick shell burning (just before point 7 in Fig. 1, $t \backsim 2.204 \times 10^7$ yr).

Core energy production by the $N^{14} \rightarrow O^{18}$ reactions is large enough to force convection near the center (see curves M_{cc} versus t and X_{18} versus t in Fig. 7). At its maximum extent during N^{14} α-burning, when $t = 2.2091 \times 10^7$ yr, the convective core occupies a mass fraction of 0.0432. The conversion of core N^{14} into O^{18} is effectively completed at $t = 2.2117 \times 10^7$ yr, at which time the core mass fraction is reduced to a relative minimum of 0.0089.

The triple-α process begins in the core even before the completion of N^{14} α-burning

(see X_{12} in Fig. 7). This accounts for the fact that the convective core begins to grow again (starting between points 8 and 9 in Fig. 1). Despite the difference in interior behavior, the evolutionary path of the 9 $M_\odot$ star in the H-R diagram appears quite similar to the paths of the 3 $M_\odot$ and 5 $M_\odot$ stars. When envelope convection becomes important (near point 10 in Fig. 1), the 9 $M_\odot$ star begins to climb steeply toward the red-giant tip, despite the existence of a core nuclear-energy source.

After the mass fraction in the growing convective core exceeds 0.0432, at $t = 2.21392 \times 10^7$ yr, N^{14} is convected inward from regions of high N^{14} abundance (see X_{18} versus t in Fig. 7). Core energy production rises sharply as a result of renewed N^{14} α-burning in the core (see L_{He}/L_H in Fig. 3 and log (L_n) in Fig. 7), which is now at higher

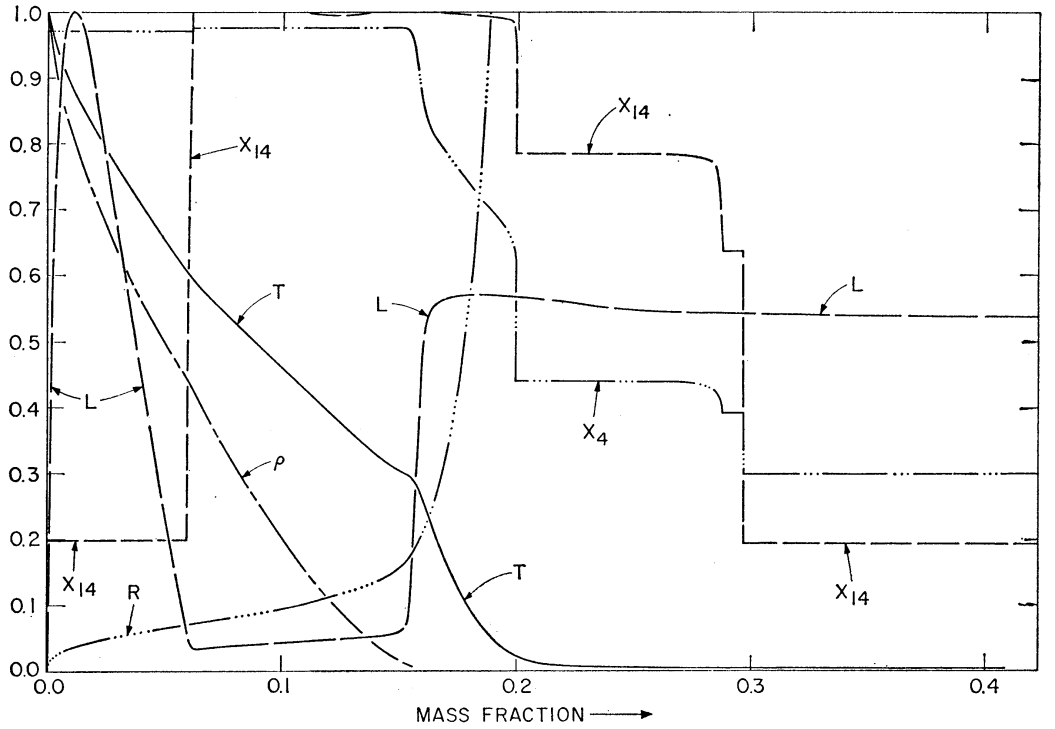

FIG. 8.—The variation with mass fraction of state and composition variables when $t = 2.21400 \times 10^7$ yr. Variables have the same significance and units as in Fig. 4. In addition, X_4 is the abundance by mass of He^4. Scale limits correspond to $0.0 \leq P \leq 309.461$, $0.0 \leq T \leq 138.418$, $0.0 \leq \rho \leq 3471.53$, $0.0 \leq L \leq 17976.4$, $0.0 \leq R \leq 175.125$, $0.0 \leq X_4 \leq 0.9757$, and $0.0 \leq X_{14} \leq 1.440 \times 10^{-2}$. The mass fraction in the static envelope is 0.0329903, and the stellar radius is $R_s = 219.673\ R_\odot$.

temperatures than during the first phase of N^{14} α-burning in the core (see log (T_c) in Fig. 7).

The distribution of characteristics within the star at $t = 2.21400 \times 10^7$ yr, when energy production in the core by the $N^{14} \rightarrow O_{18}$ reactions is near maximum, is shown in Figure 8. The extremely large rate of nuclear-energy production in the core, $L_{He} = 24663\ L_\odot$, is almost completely blanketed by absorption in the expanding core and most of the energy leaving the stellar surface, $L_s = 9427\ L_\odot$, is still supplied by the hydrogen-burning shell, $L_H = 9733\ L_\odot$. Matter *throughout* the star is cooling and expanding.

As a result of core-induced expansion, energy production in the shell decreases and (starting at point 11 in Fig. 1, $t = 2.21412 \times 10^7$ yr) the star descends rapidly in the H-R diagram until N^{14} is again reduced to nominal values in the core. It then begins (at point 12 in Fig. 1, $t = 2.21524 \times 10^7$ yr) a relatively gradual re-ascent toward the red-giant tip, which it reaches when $t = 2.22014 \times 10^7$ yr (point 13 in Fig. 1).

On reaching the red-giant tip for the second time, convection in the envelope covers the outer 76.5 per cent of the star's mass. The surface ratio of N^{14} to C^{12} is 1.27, compared to the main-sequence ratio of 0.333. This increase by a factor of 3.81 is to be compared with increases by factors of 3.26 and 2.65 in the 3 $M_\odot$ and 5 $M_\odot$ stars, respectively. The increase is largest in the 9 $M_\odot$ for several reasons. C^{12} is converted into N^{14} over a larger fraction of the interior during the phase of core hydrogen burning, and, at its maximum extent, the convective envelope reaches matter which has been enriched with N^{14} originating from the $O^{16}(p,\gamma)F^{17}(\beta^+\nu)O^{17}(p,\alpha)N^{14}$ reactions. This enrichment has occurred both during the main-sequence phase (by direct conversion) and during the shell-development stage (by convection from regions closer to the center).

V. CORE HELIUM BURNING

The descent from the red-giant tip during triple-α burning in the core (between points 13 and 15 in Fig. 1) requires 4.727×10^5 yr. As in the 3 $M_\odot$ and the 5 $M_\odot$ stars, the rate of energy production in the hydrogen-burning shell decreases during the descent (see the curve L_H versus t in Fig. 3). After reaching the relative minimum in luminosity at point 15, the mass fraction in subphotospheric convection decreases rapidly to small values (see ΔM_{CE} versus t in Fig. 7). At point 15′ ($t = 2.27231 \times 10^7$ yr) the mass fraction in the subphotospheric convective layer is 0.015 and at the position labeled CV ($t = 2.27284$) subphotospheric convection covers a mass fraction of only 0.001.

The stellar envelope undergoes an extremely rapid contraction, stellar radius decreasing from 160 $R_\odot$ to 50 $R_\odot$ in only 3150 years (see the curve of stellar radius R versus t in Fig. 7). The star traverses the path in Figure 1 between 15′ and 17 in only 4.86×10^4 yr.

Between points 15′ and 16, the increase in luminosity is supplied in part by an increase in the rate of shell energy production and in part by the release of gravitational energy from the contracting envelope (see log L versus t and log L_n versus t in Fig. 7 and L_H versus t in Fig. 3). The drop in luminosity between points 16 and 17 in Figure 1 is due to a decrease in the rate of envelope contraction as a new equilibrium between nuclear-energy production and energy transfer through the almost completely radiative envelope begins to be established.

Conditions in the star at $t = 2.27310 \times 10^7$ yr, when envelope contraction proceeds at near maximum rate, are illustrated in Figure 9. Energy production in the core by the $3\alpha \rightarrow C^{12}$ and the $C^{12}(\alpha,\gamma)O^{16}$ processes occurs at the rate $L_{He} \backsim 1413\ L_\odot$. The hydrogen-burning shell contributes at the rate $L_H \backsim 7672\ L_\odot$ and gravitational energy is released from the envelope at the rate $L_g \backsim 2041\ L_\odot$. Central abundances include $X_4 = 0.860$, $X_{12} = 0.0969$, and $X_{16} = 0.0122$. The stellar radius is 108.94 $R_\odot$ and is decreasing at the rate $dR_s/dt = 1.82 \times 10^{-2}\ R_\odot$/yr = 0.282 cm/sec. Surface temperature is increasing at the rate $dT_e/dt = 0.365°$ K/yr.

The 9 $M_\odot$ star crosses the observational Cepheid strip only once during core helium burning. If the observational strip is chosen as a linear extension of the strip defined in Figure 1 of Paper III, this crossing occurs between log $(T_e) = 3.701$ and log $(T_e) = 3.720$ and requires only 1330 yr. The passage through the Cepheid strip, which occurs as the star moves from log $(T_e) = 3.728$ to log $(T_e) = 3.709$ (in the region between points 9 and 10 in Fig. 1), requires 1010 yr. Thus, both crossings occur on a Kelvin-Helmholtz time scale.

On reaching point 18 in Figure 1 ($t = 2.31499 \times 10^7$ yr), the hydrogen-burning shell begins to enter the region defining the base of the short-lived convective layer, which was formed during the shell-development stage. The abrupt rise in hydrogen abundance in the shell accounts for the change in the nature of the path in the H-R diagram after point 18. Matter from the shell to the surface expands and the rate at which shell strength increases drops sharply (see R versus t and L_H versus t in Fig. 3).

When $t = 2.40042 \times 10^7$ yr (approximately midway between points 18 and 18′ in

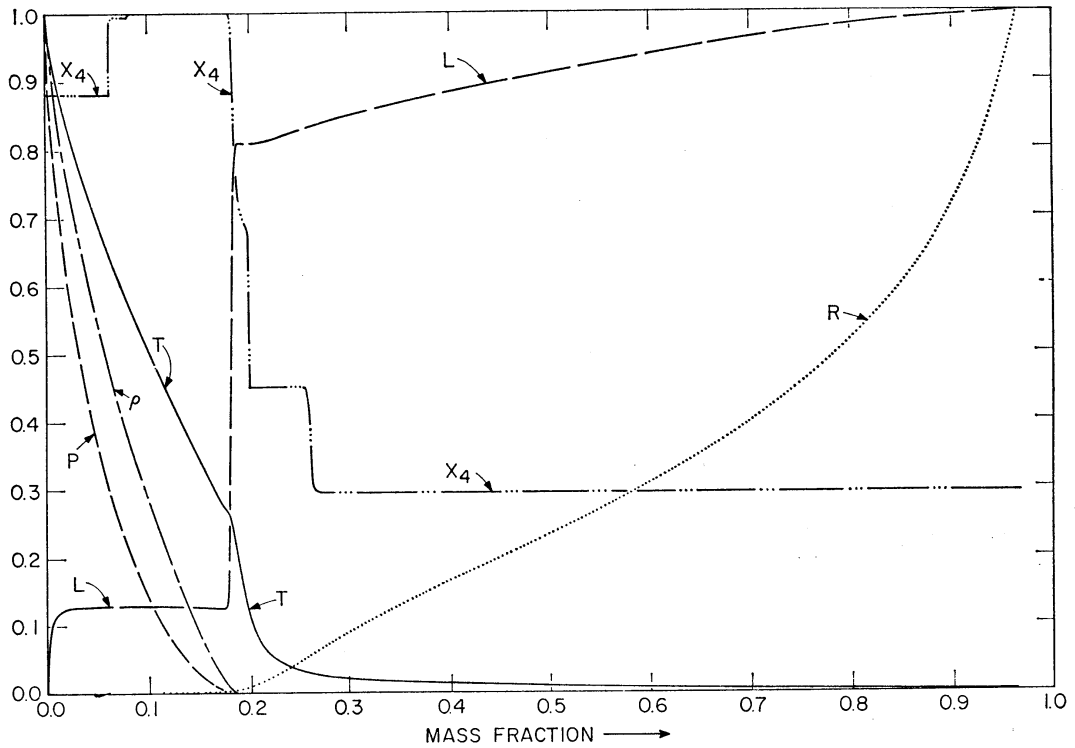

FIG. 9.—The variation with mass fraction of state and composition variables when $t = 2.27320 \times 10^7$ yr. Variables have the same significance and physical units as in Figs. 4 and 8. Scale limits correspond to $0.0 \leq P \leq 265.814$, $0.0 \leq T \leq 147.202$, $0.0 \leq \rho \leq 2845.03$, $0.0 \leq L \leq 11126.7$, $0.0 \leq R \leq 51.7129$, and $0.0 \leq X_4 \leq 0.9757$. The mass fraction in the static envelope is 0.0329903, and the stellar radius is $R_s = 108.940\ R_\odot$.

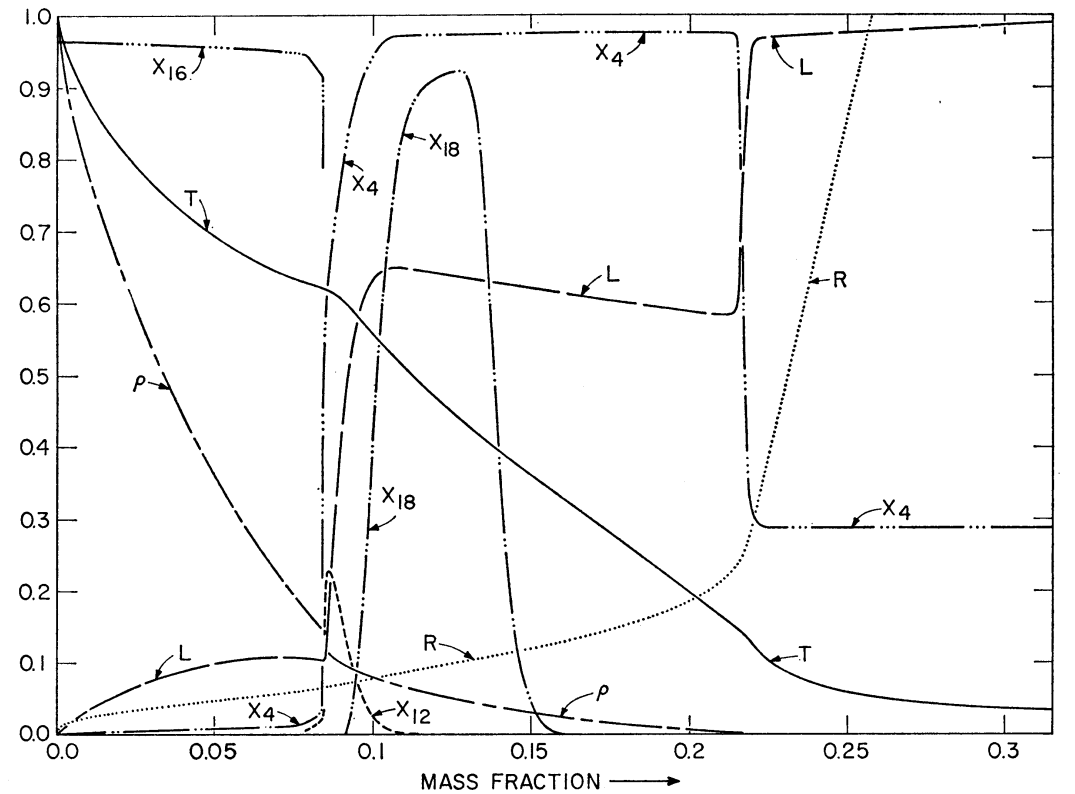

FIG. 10.—The variation with mass fraction of state and composition variables when $t = 2.62587 \times 10^7$ yr. Variables have the same significance and units as in Figs. 4 and 8. The abundance by mass of O^{18} is given by X_{18}. Scale limits correspond to $0.0 \leq T \leq 262.298$, $0.0 \leq \rho \leq 13311.9$, $0.0 \leq L \leq 16530.8$, $0.0 \leq R \leq 1.0$, $0.0 \leq X_4, X_{12}, X_{16} \leq 1.0$, and $0.0 \leq X_{18} \leq 0.02$.

Fig. 1), the envelope again begins to contract slowly, and, after point 18′, evolution is quite similar to 3 $M_\odot$ and 5 $M_\odot$ evolution at comparable stages.

In Figure 10 are shown conditions in the last model computed. From the distribution of composition characteristics, it is evident that the last vestiges of the convective layers formed during the hydrogen shell-development stage have been removed. The rate of nuclear-energy generation at the center, where $X_4 = 2.53 \times 10^{-3}$, is 0.6216 times as large as the rate of gravitational-energy release. The bulk of the energy produced between the center and the newly developed helium-burning shell ($L_{\text{core}} \backsim 1775\ L_\odot$) is contributed by the gravitational field. The energy-production rates of the helium- and hydrogen-burning shells are $L_{\text{He}} \backsim 9010\ L_\odot$ and $L_{\text{H}} \backsim 6380\ L_\odot$, respectively.

A small error has been committed by neglecting the $O^{16}(\alpha,\gamma)Ne^{20}$ reaction. At the center of the last model computed, the C^{12} and O^{16} abundances at the center are $X_{12} = 1.63 \times 10^{-4}$ and $X_{16} = 0.965$. Using the maximum off-resonant rate for the $O^{16}(\alpha,\gamma)Ne^{20}$ reaction given by Fowler and Hoyle (1964), one finds that, at the stellar center, only one α-particle is destroyed by the $O^{16}(\alpha,\gamma)Ne^{20}$ reaction for every eight which are destroyed by the $C^{12}(\alpha,\gamma)O^{16}$ reaction. Since average core temperatures have been much lower and C^{12} abundance in the core has been very much higher during the evolution preceding the last model, the neglect of the $O^{16} \rightarrow Ne^{20}$ conversion has not been at all serious.

Over the last 3×10^5 yr of computed evolution, the central temperature rises from $\backsim 2 \times 10^8$ ° K to $\backsim 2.6 \times 10^8$ ° K, corresponding to an increase in the average thermal energy per particle from 26 to 34 keV. Central helium abundance drops nearly linearly from $X_4 \backsim 0.08$ to $X_4 \backsim 2.5 \times 10^{-3}$ over this same interval. It is therefore expected that the production of neutrons for *s*-process synthesis may have occurred in the stellar core during this period via the $Ne^{22}(\alpha,n)Mg^{25}$ reaction. Ne^{22} has become available via the $O^{18}(\alpha,\gamma)Ne^{22}$ reaction. The conversion of O^{18} into Ne^{22} in the convective core is complete midway through the core helium-burning phase (see the curve X_{18} versus t in Fig. 2).

Toward the end of the evolutionary calculations, neutrino losses at the center, by electron-positron pair annihilation, are beginning to become important. Using the low-temperature approximation to the neutrino loss rate given by Fowler and Hoyle (1964), the neutrino loss rate at the center of the last model computed ($T_c = 2.623 \times 10^8$ ° K, $\rho_c = 1.331 \times 10^4$ gm/cm^3) is $\epsilon_{\nu\bar{\nu}} = -1.05 \times 10^3$ ergs gm^{-1} sec^{-1}, compared to the rate $(\epsilon_{\text{nuc}} + \epsilon_{\text{grav}})_c = 1.39 \times 10^4$ ergs gm^{-1} sec^{-1} at which energy is supplied by nuclear and gravitational sources at the center. Although only a small error has been committed here by omitting the neutrino loss rate from consideration, this loss rate will assume a non-negligible importance during further evolution.

The effect of the uncertainty in the $C^{12}(\alpha,\gamma)O^{16}$ reaction rate on the evolutionary path of the 9 $M_\odot$ star has not been explicitly calculated. However, during most of the core helium-burning phase, energy production by helium burning relative to energy production by hydrogen burning is considerably larger in the 9 $M_\odot$ star than in the 5 $M_\odot$ star. It is therefore expected that a reduction in the average surface temperature of the 9 $M_\odot$ star during core helium burning will be larger than that calculated in Paper III for the 5 $M_\odot$ star.

Special thanks are due William A. Fowler for providing spiritual and material support. Thanks are due also to G. D. McCann for supplying time on the IBM 7094 computer at the California Institute of Technology in the spring and summer of 1964.

REFERENCES

Fowler, W. A., and Hoyle, F. 1964, *Ap. J. Suppl.*, No. 91.
Iben, I., Jr. 1965*a*, *Ap. J.*, **141**, 993 (Paper I).
———. 1965*b*, *ibid.*, **142**, 1447 (Paper II).
———. 1966, *ibid.*, **143**, 483 (Paper III).